Surface-Stress-Driven Lattice Contraction Effects on the Extinction Spectra of Ultrasmall Silver Nanowires

Harold S. Park* and Xiaohu Qian

Department of Mechanical Engineering, University of Colorado, Boulder, Colorado 80309

Received: January 17, 2010; Revised Manuscript Received: April 7, 2010

We utilize numerical simulations based on the discrete dipole approximation to study the effects of surface-stress-driven lattice contraction on the extinction spectra of silver nanowires with a square cross section of length 2 nm. The novel finding of the present work is the determination that the blue shift that is induced in the silver nanowires due to surface-stress-driven lattice contraction increases with an increase in the nanowire aspect ratio; the blue shift in the longitudinal plasmon resonance wavelength reaches 20 nm in air and 30 nm in water when the nanowire aspect ratio increases to six. Furthermore, we have delineated the lattice contraction effects on the relative contributions of the free (conduction) electrons and the ionic core (bound) electrons to the observed blue shift; specifically, due to the increasingly free electron optical response of the nanowires with increasing aspect ratio, the blue shift due to the contraction-driven increase in the free electron density is found to dominate the red shift due to the increase in the core electron density for larger nanowire aspect ratios. The results collectively indicate that surface-stress-driven lattice contraction plays an important role in blue shifting the longitudinal plasmon resonance wavelength for ultrasmall silver nanowires.

Introduction

Noble metal nanostructures, particularly those made of silver and gold, have recently gained tremendous interest due to their novel optical properties. The interest in these materials has occurred because nanostructures with dimensions smaller than the wavelength of light exhibit a unique property known as surface plasmon resonance (SPR),[1−3] which occurs due to the coherent oscillation (resonance) of the conduction electrons due to the interacting electromagnetic field. These novel optical properties have led to a wealth of potential applications involving metallic nanostructures, in particular, optical sensing, detection, and imaging,[4−8] and biomedical applications based upon the specific absorption and scattering properties.[9−12]

A key development that has greatly aided the understanding of nanostructure SPR has been the recent progress in nanostructure synthesis. Many groups have demonstrated through various growth and synthesis techniques that metal nanostructures of diverse and controlled shape, size, and geometry can now be experimentally synthesized,[13−15] including recent advances in synthesizing sub-5 nm cross section metal nanowires.[16,17] In doing so, researchers have determined, both through theory and experiment, that the optical properties of metal nanostructures have a strong dependence on the nanostructure size and shape.[18−25]

An intrinsic effect that becomes significant in metallic nanostructures at sub-10 nm cross sectional sizes is that of lattice contraction that is induced by surface stresses,[26] i.e., in the absence of any externally applied force. As has been shown both experimentally[27] and using atomistic calculations,[28−31] surface stresses can cause significant elastic lattice contractions in metal nanostructures such as nanowires, with compressive strains that can easily exceed 1%; furthermore, surface stresses cause greater compressive strains as the nanowire aspect ratio increases.[29]

The deformation and lattice contraction that is induced by surface stresses are critical not only because they result in size and shape changes of the nanostructure, which are well-known to change the plasmon resonance wavelength[18,19] but also because the lattice contraction results in an increase of the electron densities, both for the ionic core and the conduction electrons; this causes additional variations in the dielectric function and thus the extinction spectra.[32,33]

The possibility that lattice contraction due to surface stresses may impact the SPR of metal nanostructures has been considered for some time, beginning with Kreibig et al.,[34,35] and continuing with more recent works.[32,33,36] However, these lattice contraction effects have not been considered in recent numerical calculations of ultrasmall metal nanostructure extinction spectra.[21,37] Furthermore, research on lattice contraction effects on the extinction spectra of metal nanostructures has focused exclusively on spherical nanoparticles.[32,33,35] The effects of lattice contraction on the extinction spectra of metal nanowires or nanorods has not, to our knowledge, been reported. Finally, it is currently unclear as to how surface-stress-driven lattice contraction effects on the conduction and core electrons couple to shift the resulting plasmon resonance wavelength.

Therefore, it is the goal of this work to quantify how lattice contraction effects resulting from surface stresses impact the extinction spectra of sub-5 nm cross section silver nanowires. We accomplish this through numerical simulations based on the discrete dipole approximation (DDA)[38] using size and lattice contraction-corrected dielectric functions for silver, where an additional feature of the present work is that the lattice contractions that occur in the silver nanowires due to surface stresses are obtained directly from accurate atomistic simulations.

Modifications of the Dielectric Function

Surface Damping Effects. In classical electrodynamic theory, the dielectric function of a material is independent of size. The bulk dielectric function is often expressed as a combination of

* To whom correspondence should be addressed. E-mail: parkhs@bu.edu.

10.1021/jp100456p
Published on Web 04/23/2010

TABLE 1: Summary of Parameters for Silver Utilized for the Surface Damping Method of Coronado and Schatz[39]

A	v_F	$1/\gamma_0$	m_{eff}
0.25[40]	1.4×10^6 m/s[24]	31×10^{-15} s[41]	$0.96m_{electron}$[41]

two terms, a Drude−Sommerfeld model for the free or conduction electrons and a core term representing the bound electrons as

$$\varepsilon_{bulk}(\omega) = \varepsilon_{core}(\omega) + \varepsilon_{free}(\omega) - 1 \quad (1)$$

where the free electron term $\varepsilon_{free}(\omega)$ is written as

$$\varepsilon_{free}(\omega) = 1 - \frac{\omega_p^2}{\omega^2 + i\gamma\omega} \quad (2)$$

and where the plasma frequency $\omega_p = (ne^2/\varepsilon_0 m_{eff})^{1/2}$ depends upon the electron density n and effective mass m_{eff}, and γ is the bulk damping constant, which is related to electron scattering processes.

However, when the size of the nanostructure becomes less than the mean free path of the conduction electrons at around 20−30 nm, the dielectric constant has been experimentally observed to deviate from the bulk value.[19,39,40] The damping constant γ_0, which is the inverse of the collision time for conduction electrons, increases because of the enhanced collision rate with the nanostructure surfaces. The size dependence of the damping constant can then be written in the form

$$\gamma(L_{eff}) = \gamma_0 + A\frac{v_F}{L_{eff}} \quad (3)$$

where A is a dimensionless parameter; v_F is the Fermi velocity; and $\gamma_0 = v_F/l_\infty$, where l_∞ is the mean free path of the conduction electrons in the corresponding bulk material and L_{eff} is the reduced effective mean free path. The parameters utilized in the present calculations for silver are summarized in Table 1.

Coronado and Schatz[39] have developed a geometric probability approach to calculate L_{eff} for nanostructures of various shapes and sizes, resulting in the analytic expression

$$L_{eff} = 4\frac{V}{S} \quad (4)$$

where S is the surface area and V is the volume of the nanostructure. The damping that occurs due to the reduced mean free path is assumed to act solely on the conduction electrons; therefore, the modified bulk dielectric constant in eq 1 is written as[39,40]

$$\varepsilon_{bulk}(\omega) = \varepsilon_{core}(\omega) + 1 - \frac{\omega_p^2}{\omega^2 + i\omega\left(\gamma_0 + A\frac{v_F}{L_{eff}}\right)} \quad (5)$$

Lattice Contraction Effects. In addition to surface damping, lattice contraction effects due to deformation induced by surface stresses[30,31] must also be included in the dielectric function of both the core and conduction (free) electrons. For the conduction electrons, we follow the work of Cai et al.,[33] who noted that due to the lattice contraction the plasma frequency ω_p in eq 2 changes due to the resulting increase in free electron density; the plasma frequency can be written for FCC metals as

$$\omega_p^2 = \frac{4e^2}{\varepsilon_0 m_{eff} a_0^2(a_0 - \Delta a)} \quad (6)$$

where e is the electric charge; $a_0 = 4.09$ Å is the undeformed lattice constant; and Δa is the decrease in lattice constant due to deformation induced by surface stresses. Clearly, a decrease in lattice constant a_0 due to lattice contraction will increase the plasma frequency ω_p, resulting in a blue shift of the extinction spectra.

We note that the expression in eq 6 differs from that given in Cai et al.;[33] this is because Cai et al. considered spherical nanoparticles in which the lattice contraction occurs symmetrically. In contrast for nanowires, as will be demonstrated in the numerical results, the surface stresses cause deformation predominately in the axial direction, while the transverse directions of the nanowires are comparably undeformed. Therefore, the modified expression in eq 6 assumes that the nanowire deforms due to surface stresses in the axial direction only.

Furthermore, the decrease in lattice constant a_0 also impacts the Fermi velocity v_F in eqs 3 and 5; this is because the Fermi energy can be written as

$$E_F = \frac{h^2}{2m}\left(\frac{3}{8\pi}\right)^{2/3} N^{2/3} \quad (7)$$

where h is Planck's constant; m is the electron mass; and N is the number of free electrons per volume (electron density). Because the electron density N can be written as, for FCC metals, again accounting for the fact that surface stresses cause predominately axial deformation in metal nanowires

$$N = \frac{4}{a_0^2(a_0 - \Delta a)} \quad (8)$$

and noting that the Fermi velocity can be written in terms of the Fermi energy as

$$v_F = \sqrt{\frac{2E_F}{m}} \quad (9)$$

it is evident that a decrease in the lattice constant a_0 will increase the Fermi velocity v_F due to an increase in the Fermi energy E_F.

However, as discussed by Lerme et al.,[32] the lattice contraction not only affects the dielectric function of the free, or conduction, electrons but also affects the dielectric function for the ionic core, or bound, electrons. This can be written as

$$\varepsilon_{\text{core}}(\omega) \rightarrow \frac{\varepsilon_{\text{core}}(\omega) + 2 + 2\nu(\varepsilon_{\text{core}}(\omega) - 1)}{\varepsilon_{\text{core}}(\omega) + 2 - \nu(\varepsilon_{\text{core}}(\omega) - 1)} \quad (10)$$

where the constant ν captures the effects of the lattice contraction as

$$\nu = \left(\frac{a_0}{a_0 - \Delta a}\right) \quad (11)$$

Again, we note that the expression given in eq 11 differs from that of Lerme et al.[32] due to the fact that we have considered shape changes in nanowires, which occur predominately along the axial direction, as compared to spherically symmetric lattice contraction that occurs in spherical nanoparticles.

We note that the correction to the dielectric function for the ionic core electrons in eq 10 is based upon classical theories, which neglect quantum effects such as electron spill out that lead to a blue shift in small metal nanostructures[42] with decreasing size. In other words, in quantum models due to the spillout effect, fewer electrons are inside the nanowire, and therefore fewer electrons are subject to the lattice contraction effects on $\varepsilon_{\text{core}}(\omega)$ in eq 10. The net effect of neglecting the spill out is that the red shift that results from the classical model in eq 10 will be larger than that which would occur using a quantum model. However, we will demonstrate that despite the overprediction in red shift which occurs due to this model at very small nanostructure sizes the red shift is small compared to strain effects on the blue shift due to the free electron effect and becomes less important with increasing nanowire aspect ratio.

In summary, the final classical dielectric function including effects from surface damping,[39] lattice contraction effects on the free electron density,[33] and lattice contraction effects on the ionic core[32] can be found by combining eqs 5, 6, and 10; further details can be found in the work of Qian and Park.[43]

Numerical Methodology

To calculate the extinction spectra of the silver nanowires, we utilize the discrete dipole approximation (DDA),[38] which was originally developed by Purcell and Pennypacker. The fundamental idea behind the DDA is to discretize a volume of arbitrary geometry using small (finite) elements, in which each element represents an individual dipole with polarizability α_i that interacts, due to an incident electric field, with all other dipoles in the body. The polarization can be written as[20]

$$\mathbf{P}_i = \alpha_i \mathbf{E}_{\text{loc}}(\mathbf{r}_i) \quad (12)$$

where the local electric field $\mathbf{E}_{\text{loc},i}$ is the sum of an incident field $\mathbf{E}_{\text{inc},i}$ and the contribution from the j other dipoles in the system $\mathbf{E}_{\text{other},j}$ and can be written as

$$\mathbf{E}_{\text{loc},i} = \mathbf{E}_{\text{inc},i} + \mathbf{E}_{\text{other},j} = \mathbf{E}_0 \exp(i\mathbf{k}\cdot\mathbf{r}_i) - \sum_{j\neq i} \mathbf{A}_{ij}\cdot\mathbf{P}_j \quad (13)$$

where $\mathbf{k}$ is the wave vector of the incident plane wave; $\mathbf{E}_0$ is the amplitude of the plane wave; and the matrix $\mathbf{A}_{ij}$ represents the interactions of all dipoles i and j as

$$\mathbf{A}_{ij}\cdot\mathbf{P}_j = \frac{\exp(ik\mathbf{r}_{ij})}{\mathbf{r}_{ij}^3}\left(k^2\mathbf{r}_{ij}\times(\mathbf{r}_{ij}\times\mathbf{P}_j) + \frac{1 - ik\mathbf{r}_{ij}}{\mathbf{r}_{ij}^2}\times(\mathbf{r}_{ij}^2\mathbf{P}_j - 3\mathbf{r}_{ij}(\mathbf{r}_{ij}\cdot\mathbf{P}_j))\right) \quad (14)$$

The goal of the DDA method is to solve for the polarization vector $\mathbf{P}$ in eq 13. Once this is performed, the extinction cross section can be calculated as[44]

$$C_{\text{ext}} = \frac{4\pi k}{|\mathbf{E}_0|^2}\sum_{j=1}^{N} \text{Im}(\mathbf{E}^*_{\text{inc},j}\cdot\mathbf{P}_j) \quad (15)$$

In the present work, we calculate the extinction spectra using the code DDScat[45] by Draine and Flatau; this code has recently been utilized by various authors[10,18,20,21,24,25,39] to study the extinction spectra of metallic nanostructures.

Results

The DDA calculations were performed on silver nanowires with a square cross section of length 2.045 nm and aspect ratios ranging between one and six. The calculations required between 125 000 and 257 250 dipoles to discretize the nanowires; we utilized a minimum of 35 dipoles across the nanowire cross section in each direction to ensure that the nanowire was sufficiently discretized. We note that this discretization implies that the dipole spacing is about 1 order of magnitude smaller than the lattice spacing of silver, which is 4.09 Å. Therefore, concerns may be raised considering the validity of the present DDA results.

However, we note that the dipoles that are used to discretize the nanowire volume are not required to correspond to actual atomic positions and furthermore do not represent individual atoms. For example, dipole discretizations that are much larger than the lattice spacing can be used and in fact are predominately used in the DDA calculations that are found in the literature; such discretizations would also be physically unreasonable if the dipoles were constrained to represent individual atoms. Similarly, dipole spacings smaller than the lattice spacing have also been utilized in previous works based upon the DDA.[24,25,37] In these works, as well as in this article, the choice of a dipole spacing that is smaller than the lattice spacing is made to ensure convergence of the numerical simulations.

The nanowire geometries were created as follows. First, nanowires were formed with atoms at their bulk lattice positions assuming a ⟨100⟩ axial orientation and {100} transverse surfaces. We then used molecular statics simulations[46] using an embedded atom (EAM) potential for silver[47] to determine the minimum energy configurations of the nanowires due to surface stresses, i.e., in the absence of any externally applied forces; we emphasize that EAM potentials are known to give accurate qualitative values for the surface energies and surface stresses for metallic surfaces.[48]

The surface stresses are intrinsic to nanostructures; they occur due to the fact that surface atoms have fewer bonding neighbors than do atoms that lie within the material bulk.[26,49] Because of this lack of bonding coordination, the surface atoms are subject to a surface stress that is tensile in metal nanowires, which implies that the nanowire could reduce its surface energy by contracting. Therefore, at equilibrium as shown in Figure 1, the tensile surface stress is balanced by the compressive stress within

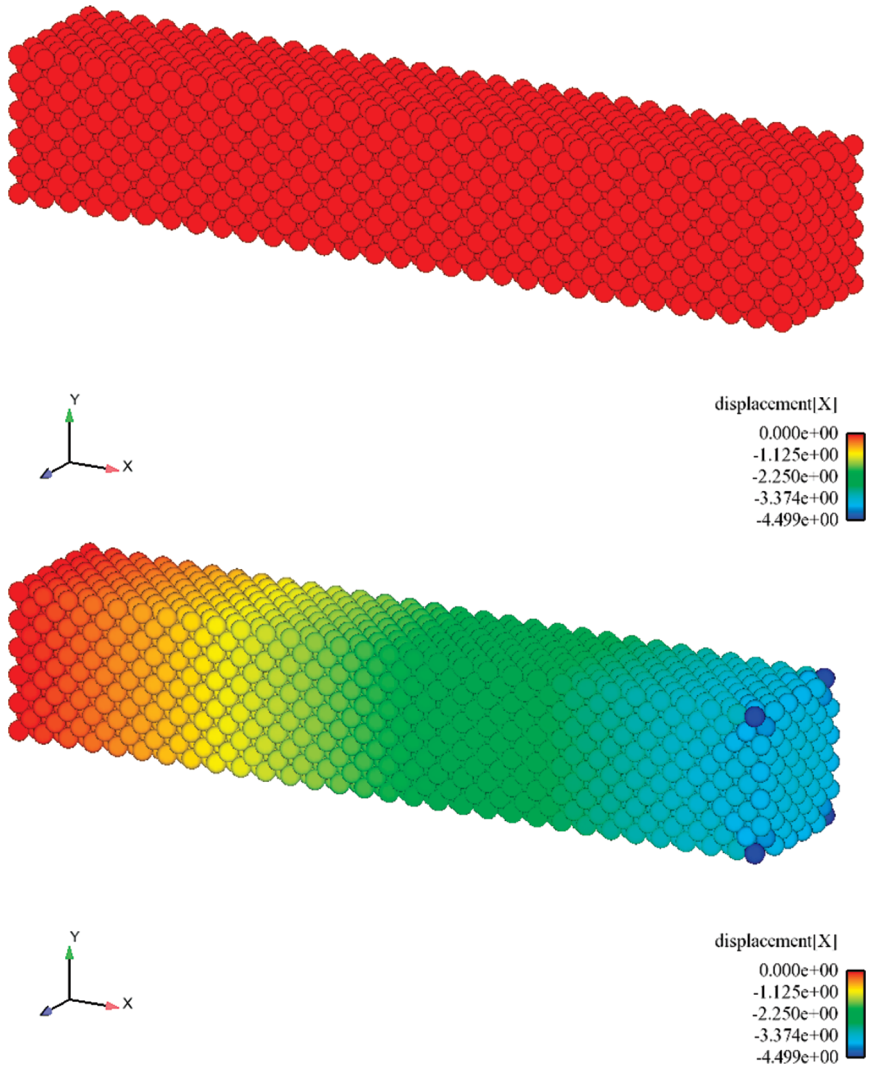

Figure 1. Surface stress driven compression of 12.27 × 2.045 × 2.045 nm silver nanowire. (Top): initial, undeformed silver nanowire with axial length of 12.27 nm. (Bottom): equilibrium configuration of a deformed silver nanowire with axial length of 11.9224 nm, corresponding to a compression of 2.83% due to surface stresses.

the nanowire core that results from the overall state of compression the nanowires undergo due to the surface stresses.

Figure 1 shows images of both the undeformed ("bulk") nanowire with bulk lattice positions and also the equilibrium configuration of the nanowire after compressive deformation ("contract") due to surface stresses; we note the homogeneous state of compressive strain caused by the surface stresses in the nanowire. It is clear that the deformation induced by surface stresses for the silver nanowire with a cross sectional length of 2.045 nm is substantial, and the compressive strains induced by the surface stresses increase from 1.79% for a nanowire with cubic dimensions of length 2.045 nm to 2.92% for a nanowire with aspect ratio of six as shown in Table 2. Furthermore, the deformation is entirely elastic; i.e., no defects or dislocations are generated due to the nanowire contraction. The original (bulk) nanowire geometries and the resulting geometries after surface-stress-driven axial compression (contract) are shown in Table 2; the transverse expansion of the nanowires during surface-stress-driven compression is neglected as it is less than 1% of the axial compression.

For the bulk geometries in Table 2, we calculated the extinction spectra using the optical properties for silver given by Johnson and Christy[41] modified using the surface damping correction of Coronado and Schatz;[39] these calculations were performed with the goal of quantifying the errors that would be introduced in simulations of the extinction spectra of ultrasmall metal nanowires by neglecting lattice contraction effects due to surface stresses. The extinction spectra were calculated in this work for all geometries for the longitudinal resonance mode only.

TABLE 2: Comparison of Dimensions of Bulk Silver Nanowires, Where Deformation Due to Surface Stresses Is Neglected, and Nanowires That Contract Axially Due to Surface Stresses[a]

bulk	contract	strain
2.045 × 2.045 × 2.045	2.00846 × 2.045 × 2.045	−1.79%
4.09 × 2.045 × 2.045	3.99033 × 2.045 × 2.045	−2.44%
8.18 × 2.045 × 2.045	7.95651 × 2.045 × 2.045	−2.73%
12.27 × 2.045 × 2.045	11.9224 × 2.045 × 2.045	−2.92%

[a] All dimensions are in nm.

For the contract geometries in Table 2, we calculated the longitudinal plasmon resonance peak using three sets of optical constants. First, we utilized the optical constants of Johnson and Christy[41] modified using the surface damping of Coronado and Schatz.[39] We note that due to geometric changes that occur between the bulk and contract geometries in Table 2 the surface damping effect, i.e., L_{eff} in eq 3, is slightly modified. Second,

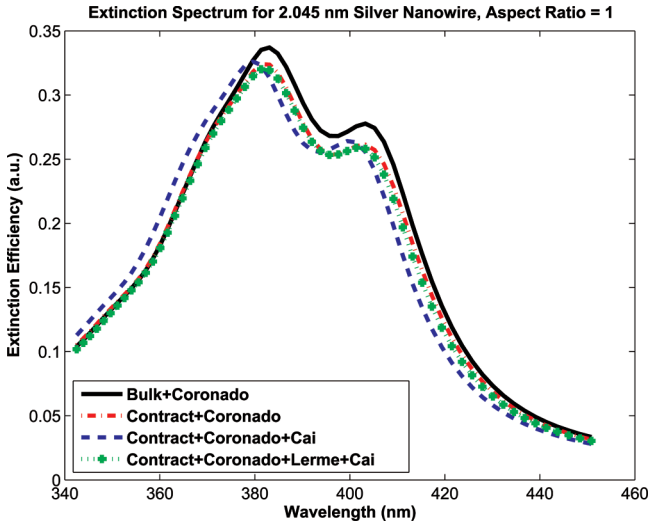

Figure 2. Extinction spectra for 2.045 nm silver nanowires in air with an aspect ratio of one.

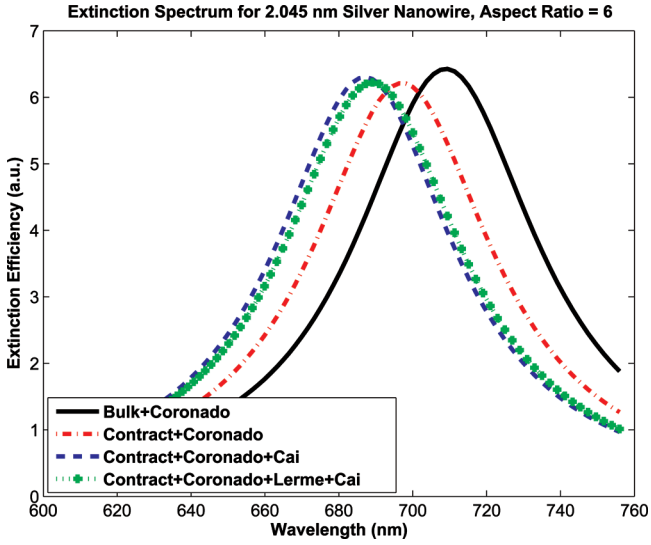

Figure 3. Extinction spectra for 2.045 nm silver nanowires in air with an aspect ratio of six.

we included both surface damping and lattice contraction effects on the dielectric function of the free electrons using eqs 6−9; this was done to determine the effects of ignoring lattice contraction on the ionic core dielectric function, as was done by Cai et al.[33] Finally, we included all effects: surface damping,[39] free electron dielectric changes due to lattice contraction,[33] and ionic core electron dielectric changes due to lattice contraction effects.[32]

The extinction spectra for the 2.045 nm square cross section silver nanowires with aspect ratios of one and six are shown in Figure 2 and Figure 3, while the blue or red shifts that are induced by the various factors under consideration (shape changes and changes to dielectric functions of core and free electrons) are shown in Figure 4. We first note that the longitudinal plasmon resonance wavelength red shifts with increasing nanowire aspect ratio and that the extinction maxima increases with increasing nanowire aspect ratio; such results have been observed in previous parametric investigations of metal nanorods.[21,20] For the "bulk" geometry in Table 2, the longitudinal plasmon resonance peak red shifts from $\lambda = 383$ nm for the cubic nanowire to $\lambda = 709$ nm for a nanowire with an aspect ratio of six. Furthermore, except for the quadrupole mode

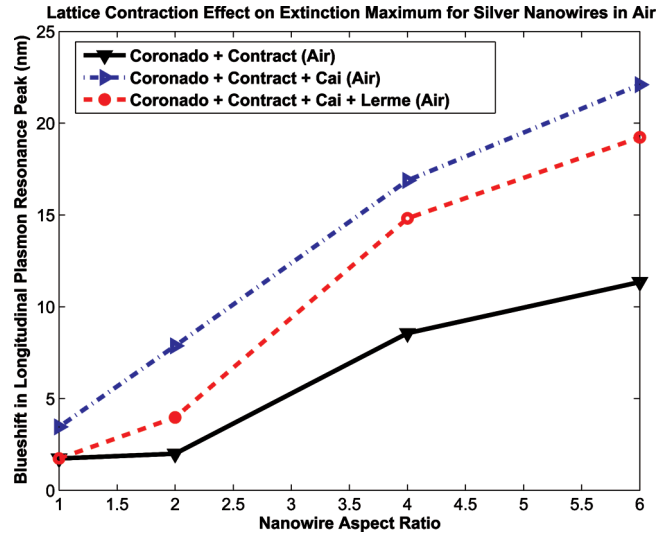

Figure 4. Blue shift of the longitudinal plasmon resonance peak for 2.045 nm silver nanowires in air due to lattice contraction effects.

observed at $\lambda = 403$ nm for the cubic nanowire in Figure 2, higher-order plasmon resonant modes are not observed.

Another trend that is clear is that if shape changes due to lattice contraction are accounted for, as illustrated in Table 2, there is a distinct blue shift that occurs with increasing aspect ratio; as shown in Figure 4, the blue shift due solely to shape changes from surface-stress-induced lattice contraction (contract + coronado) increases from 1.74 nm for a cubic nanowire to more than 11 nm when the nanowire aspect ratio is six. The increase in blue shift for increasing nanowire aspect ratio likely occurs due to the increase in compressive strain that is induced by the surface stresses with increasing aspect ratio as seen in Table 2.

Figure 2 and Figure 3 also demonstrate another significant point, which is in the competing effects of lattice contraction, i.e., the blue shift that is induced by the increase in plasma frequency ω_p of the free electrons and the red shift that is induced by an increase in the density of the core electrons.[32] As seen in Figure 2 and Figure 3, and further quantified in Figure 4, accounting for lattice contraction effects on the free electrons alone (contract + coronado + cai) leads to an increasing blue shift with increasing nanowire aspect ratio, from about 3.5 nm for the cubic nanowire to more than 22 nm when the nanowire aspect ratio increases to six.

However, as seen in Figure 2 and Figure 3 and further quantified in Figure 4, when the lattice contraction effects on the ionic core dielectric function are accounted for (contract + coronado + lerme + cai), a slight red shift that varies from about 2 to 4 nm as compared to when lattice contraction effects are accounted for only on the free electrons is observed. However, this red shift is clearly smaller than the blue shift induced by the increase in plasma frequency of the free electrons, and therefore when all effects are accounted for (surface damping, shape changes due to lattice contraction, and dielectric function changes due to lattice contraction to both the free and core electrons), the blue shift in longitudinal plasmon resonance wavelength increases from about 2 nm for the cubic nanowire to about 20 nm when the nanowire aspect ratio is six.

To quantify the effect of the surrounding dielectric medium on the blue shift due to lattice contraction, we performed the DDA calculations for the silver nanowires in water ($n = 1.34$); similar to the case of the silver nanowires in air shown in Figure

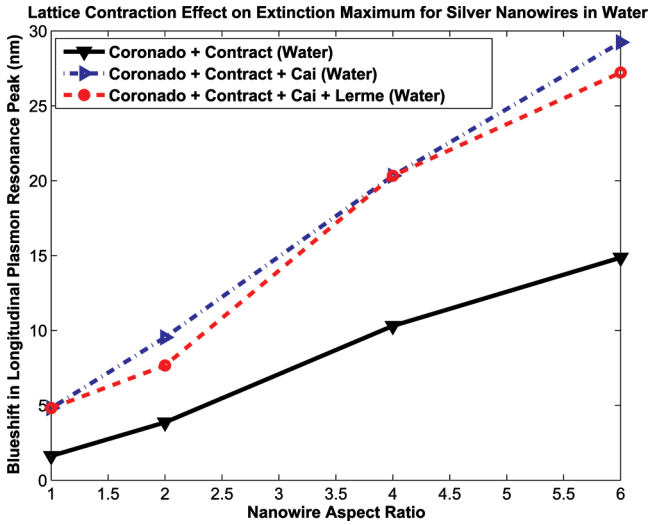

Figure 5. Blue shift of longitudinal plasmon resonance peak for 2.045 nm silver nanowires in water due to lattice contraction effects.

4, we quantify the effects of both geometric changes and lattice contraction effects on both the core and free electron dielectric functions for silver nanowires in water in Figure 5. It is evident from Figure 5 that not only does water enhance the blue shifts due to an increase in the free electron density as compared to nanowires in air but also the red shifts due to an increase in the core electron density are suppressed as compared to nanowires in air in Figure 4. Therefore, including all effects (shape changes and dielectric function changes due to lattice contraction), the blue shift increases from about 5 nm for the cubic 2.045 nm nanowire to nearly 30 nm when the nanowire aspect ratio increases to six.

Figure 4 and Figure 5 also demonstrate another point that we wish to emphasize. In particular, both figures show that, regardless of the surrounding dielectric medium, the blue shift that is predicted solely due to shape changes caused by surface-stress-induced lattice contraction (coronado + contract in Figure 4 and Figure 5) is only about 50% of the total blue shift (coronado + contract + cai + lerme); this shows that a significant underprediction of the lattice contraction induced blue shift would occur if the effects of lattice contraction on both the core and free electron dielectric functions are not accounted for.

We now address the question as to why the blue shift due to lattice contraction effects on the free electrons dominates the red shift due to lattice contraction effects on the core electrons. Specifically, this occurs because the interband transitions in silver occur around $\lambda = 330$ nm, or at an incident photon energy of about 3.74 eV.[41] Therefore, for photon energies greater than about 3.74 eV, or wavelengths less than $\lambda = 330$ nm, the interband transitions, and therefore the effects of the core electrons, dominate the optical response. However, the longitudinal plasmon resonant frequencies observed in the present work range were observed at wavelengths ranging from $\lambda = 383$ to 709 nm; all of these therefore occur at energies or wavelengths where the free electron response dominates, thus leading to the net blue shift due to lattice contraction that we have observed.

Discussion

We now compare and discuss the present results within the context of previous theoretical results that considered lattice contraction effects on the SPR of silver nanoparticles.[32,33] We first note that the small blue shift of 2 nm (5 nm in water) that we found due to lattice contraction for the cubic nanowires is similar to that reported by Lerme et al.[32] for spherical silver nanoparticles, in which the blue shift due to an increase in plasma frequency for the conduction electrons essentially canceled the red shift due to an increase in electron density for the core electrons. Again, as discussed by Lerme et al.,[32] this blue shift is smaller than that which is found using quantum calculations due to the fact that the electron spillout effect is not considered; in essence, because the spillout effect is neglected within the classical approximation, more core electrons are subject to the lattice contraction than should be, thus leading to a slightly exaggerated red shift.

However, the effects of lattice contraction for nonspherical nanostructures was not considered by Lerme et al.;[32] we have demonstrated in the present work that the blue shift due to lattice contraction increases with increasing nanowire aspect ratio and that the red shift due to lattice contraction effects on the core electrons is relatively small (no larger than 4 nm) for all aspect ratios. This finding bolsters the qualitative credibility of the current results, which were based upon classical approximations to the dielectric functions, for multiple reasons. First, it was found by Lerme et al.[32] that if lattice contraction effects were accounted for on the free electrons only that the blue shift trend that resulted from this classical prediction matched that from quantum predictions for ultrasmall silver clusters as a function of decreasing cluster size, while the absolute value of the blue shift was underpredicted. Second, discrepancies between the quantum calculations and classical calculations based solely on the enhancement in free electron density due to lattice contraction were found to decrease significantly for nanoparticle diameters larger than 1 nm due to the decreasing importance of electron spillout effects with increasing nanoparticle size.

On the basis of these comparisons, the results obtained in Figure 4 and Figure 5 are physically reasonable, while also suggesting that the total blue shift we have calculated is likely to be slightly underpredicted by the classical model we have utilized. We arrive at this conclusion because regardless of whether lattice contraction effects on only the free electrons or both the free and bound electrons are considered we see in Figure 4 and Figure 5 that an almost linear increase in the blue shift with increasing aspect ratio is predicted. Furthermore, the red shift due to lattice contraction effects on the core electrons, which is known to be overpredicted by classical theories for small nanostructures, is still relatively small.

We also compare results to those obtained by Cai et al.,[33] who studied lattice contraction effects on silver nanoparticles, but accounted only for the effects of lattice contraction on the free electrons. In that work, a blue shift of 0.17 eV was found for free-standing silver nanoparticles with a 2 nm diameter in vacuum. In contrast, the largest blue shift found in the present work is about 0.06 eV for the silver nanowire with an aspect ratio of four, which is considerably smaller. The differences between the present results and those of Cai et al. are likely due to the following reasons. First, for spherical nanoparticles, the lattice contraction occurs symmetrically, i.e., in all three directions. This is in contrast to the presently studied nanowires, where the lattice contraction occurs in only one direction, i.e., in the axial direction of the nanowire; as seen in eqs 6 and 11, the net change in plasma frequency ω_p and the core dielectric function ε_{core} will correspondingly be smaller for nanowires than nanoparticles. Because of this, nanowires show a smaller blue shift for the same amount of lattice contraction induced strain as a nanoparticle. Second, the lattice contraction in the present

work was obtained directly from atomistic simulations; for the 2 nm cubic nanowire, a lattice contraction of about 1.8% was obtained. In contrast, Cai et al. predicted a lattice contraction of more than 4.5% for a 2 nm silver nanoparticle using analytic expressions. Therefore, the combination of the differences in nanostructure geometry and the reduced strain due to lattice contraction leads to the smaller blue shifts due to lattice contraction in the present work as compared to the work of Cai et al.

We also discuss the issue of nonlocal effects, which have recently been used to study the optical properties of ultrasmall metal nanostructures.[50−54] The nonlocal effects are accounted for by making the dielectric function ε dependent not only on the angular frequency ω, as in eq 1, but also on the wave vector **k**, and physically account for various nanoscale effects, namely, electron spillout effects and quantum confinement/surface damping effects.[54] The nonlocal effects have been shown to lead to significant reductions in the extinction efficiency and blue shifts in the plasmon resonance wavelength.[50,54] For example, McMahon et al.[50] showed that nonlocal effects introduce an inherent blue shift in the plasmon resonance wavelength of 4 nm diameter gold nanorods of nearly 0.01 eV; similar blue shifts in the plasmon resonance wavelength of individual gold nanoparticles were observed experimentally by Palomba et al.[53]

The classical calculations and dielectric functions we have utilized in the present work do not explicitly account for nonlocal effects in that the dielectric functions are independent of the wave vector **k**, though surface damping effects are accounted for classically using the approach of Coronado and Schatz.[39] In general, the blue shifts due to surface-stress-driven lattice contraction that we have calculated in the present work appear to be larger than the blue shifts due to the nonlocal effects; i.e., the strain-driven blue shifts are on the order of 0.05 eV, while the blue shifts due to nonlocal effects were reported by McMahon et al.[50] to be on the order of 0.01 eV, with the caveat that the nonlocal results were obtained for gold, and not silver, nanowires as we have considered in the present work. Overall, it appears likely that the lattice contraction effects we have reported here may augment the nonlocal effects reported elsewhere, thus leading to even larger blue shifts for ultrasmall silver nanowires than what we have reported here.

We also discuss the relevance of the nanowire axial orientation on the results we have obtained. Specifically, recent MD simulations have shown that ⟨100⟩ FCC metal nanowires undergo more surface-stress-driven lattice contraction than do nanowires that have ⟨110⟩ and ⟨111⟩ orientations.[28] Therefore, it is likely that a smaller blue shift would be observed due to surface-stress-driven lattice contraction for ⟨110⟩ and ⟨111⟩ FCC metal nanowires.

We close by noting that we have not directly compared the results obtained in the present work to other previous experimental studies on the optical properties of ultrasmall metal nanoparticles.[40,42,55−58] This is mainly because without knowing the exact lattice constants due to surface-stress-driven lattice contraction for the metal nanostructures that have been studied experimentally it is difficult to directly ascribe blue or red shifts that have been observed experimentally to lattice contraction effects. Therefore, we have focused in the present work on isolating and understanding the effects of surface-stress-induced lattice contraction on the optical properties of ultrasmall silver nanowires.

Conclusions

We have utilized classical electrodynamics simulations based upon the discrete dipole approximation to study surface-stress-induced lattice contraction effects on the extinction spectra of 2 nm silver nanowires. By accounting for lattice contraction effects using classical approximations on both the conduction (free) electrons and the ionic core (bound) electrons, we find a blue shift that increases nearly linearly with increasing nanowire aspect ratio. Furthermore, we found that the blue shift due to the increase in free electron density dominates the red shift due to an increase in the core electron density due to the fact that the extinction maxima for all nanowires occur at wavelengths that do not coincide with the interband transition energy for silver.

Acknowledgment. H.S.P. and X.H.Q. gratefully acknowledge support from the NSF, grant CMMI-0750395, as well as help from Bruce T. Draine with using the DDScat code.

References and Notes

(1) Ozbay, E. *Science* **2006**, *311*, 189–193.
(2) Sambles, J. R.; Bradbery, G. W.; Yang, F. *Contemp. Phys.* **1991**, *32*, 173–183.
(3) Barnes, W. L.; Dereux, A.; Ebbeson, T. W. *Nature* **2003**, *424*, 824–830.
(4) Mock, J. J.; Oldenburg, S. J.; Smith, D. R.; Schultz, D. A.; Schultz, S. *Nano Lett.* **2002**, *2*, 465–469.
(5) Nicewarner-Pena, S. R.; Freeman, R. G.; Reiss, B. D.; He, L.; Pena, D. J.; Walton, I. D.; Cromer, R.; Keating, C. D.; Natan, M. J. *Science* **2001**, *294*, 137–141.
(6) Han, M.; Gao, X.; Su, J. Z.; Nie, S. *Nat. Biotechnol.* **2001**, *19*, 631–635.
(7) Sokolov, K.; Follen, M.; Aaron, J.; Pavlova, I.; Malpica, A.; Lotan, R.; Richards-Kortum, R. *Cancer Res.* **2003**, *63*, 1999–2004.
(8) Stone, J. W.; Sisco, P. N.; Goldsmith, E. C.; Baxter, S. C.; Murphy, C. J. *Nano Lett.* **2007**, *7*, 116–119.
(9) Hirsch, L. R.; Stafford, R. J.; Bankson, J. A.; Sershen, S. R.; Rivera, B.; Price, R. E.; Hazle, J. D.; Halas, N. J.; West, J. L. *Proc. Natl. Acad. Sci.* **2003**, *100*, 13549–13554.
(10) Jain, P. K.; Lee, K. S.; El-Sayed, I. H.; El-Sayed, M. A. *J. Phys. Chem. B* **2006**, *110*, 7238–7248.
(11) Hirsch, L. R.; Gobin, A. M.; Lowery, A. R.; Tam, F.; Drezek, R. A.; Halas, N. J.; West, J. L. *Ann. of Biomed. Eng.* **2006**, *34*, 15–22.
(12) Anker, J. N.; Hall, W. P.; Lyandres, O.; Shah, N. C.; Zhao, J.; Duyne, R. P. V. *Nat. Mater.* **2008**, *7*, 442–453.
(13) Wiley, B.; Sun, Y.; Mayers, B.; Xia, Y. *Chem.—Eur. J.* **2005**, *11*, 454–463.
(14) Sun, Y.; Xia, Y. *Analyst* **2003**, *128*, 686–691.
(15) Murphy, C. J.; Jana, N. R. *Acta Mater.* **2002**, *14*, 80–82.
(16) Huo, Z.; Tsung, C.-K.; Huang, W.; Zhang, X.; Yang, P. *Nano Lett.* **2008**, *8*, 2041–2044.
(17) Lu, X.; Yavuz, M. S.; Tuan, H.-Y.; Korgel, B. A.; Xia, Y. *J. Am. Chem. Soc.* **2008**, *130*, 8900–8901.
(18) Kelly, K. L.; Coronado, E.; Zhao, L. L.; Schatz, G. C. *J. Phys. Chem. B* **2003**, *107*, 668–677.
(19) Link, S.; El-Sayed, M. A. *J. Phys. Chem. B* **1999**, *103*, 8410–8426.
(20) Lee, K.-S.; El-Sayed, M. A. *J. Phys. Chem. B* **2005**, *109*, 20331–20338.
(21) Prescott, S. W.; Mulvaney, P. *J. Appl. Phys.* **2006**, *99*, 123504.
(22) Aizpurua, J.; Bryant, G. W.; Richter, L. J.; de Abajo, F. J. G.; Kelley, B. K.; Mallouk, T. *Phys. Rev. B* **2005**, *71*, 235420.
(23) Bryant, G. W.; de Abajo, F. J. G.; Aizpurua, J. *Nano Lett.* **2008**, *8*, 631–636.
(24) Felidj, N.; Aubard, J.; Levi, G. *J. Chem. Phys.* **1999**, *111*, 1195–1208.
(25) Hao, E.; Schatz, G. C. *J. Chem. Phys.* **2004**, *120*, 357–366.
(26) Cammarata, R. C. *Prog. Surf. Sci.* **1994**, *46*, 1–38.
(27) Huang, W. J.; Sun, R.; Tao, J.; Menard, L. D.; Nuzzo, R. G.; Zuo, J. M. *Nat. Mater.* **2008**, *7*, 308–313.
(28) Liang, H.; Upmanyu, M.; Huang, H. *Phys. Rev. B* **2005**, *71*, 241403(R).
(29) Park, H. S.; Klein, P. A. *Phys. Rev. B* **2007**, *75*, 085408.
(30) Park, H. S.; Gall, K.; Zimmerman, J. A. *Phys. Rev. Lett.* **2005**, *95*, 255504.
(31) Diao, J.; Gall, K.; Dunn, M. L. *Nat. Mater.* **2003**, *2*, 656–660.
(32) Lerme, J.; Pellarin, M.; Cottancin, E.; Gaudry, M.; Broyer, M.; Fatti, N. D.; Vallee, F.; Voisin, C. *Eur. Phys. J. D* **2001**, *17*, 213–220.
(33) Cai, W.; Hofmeister, H.; Dubiel, M. *Eur. Phys. J. D* **2001**, *13*, 245–253.
(34) Kreibig, U.; Genzel, L. *Surf. Sci.* **1985**, *156*, 678–700.

(35) Kreibig, U.; Vollmer, M. *Optical properties of metal clusters*; Springer-Verlag, 1995.
(36) Dalacu, D.; Martinu, L. *J. Opt. Soc. Am. B* **2001**, *18*, 85–92.
(37) Brioude, A.; Jiang, X. C.; Pileni, M. P. *J. Phys. Chem. B* **2005**, *109*, 13138–13142.
(38) Purcell, E. M.; Pennypacker, C. R. *Astrophys. J.* **1973**, *1986*, 705–714.
(39) Coronado, E. A.; Schatz, G. C. *J. Chem. Phys.* **2003**, *119*, 3926–3934.
(40) Hovel, H.; Fritz, S.; Hilger, A.; Kreibig, U.; Vollmer, M. *Phys. Rev. B* **1993**, *48*, 18178–18188.
(41) Johnson, P. B.; Christy, R. W. *Phys. Rev. B* **1972**, *6*, 4370–4379.
(42) Liebsch, A. *Phys. Rev. B* **1993**, *48*, 11317–11328.
(43) Qian, X.-H.; Park, H. S. *J. Mech. Phys. Solids* **2010**, *58*, 330–345.
(44) Draine, B. T.; Flatau, P. J. *J. Opt. Soc. Am. A* **1994**, *11*, 1491–1499.
(45) Draine, B. T.; Flatau, P. J. http://arxiv.org/abs/0809.0337, 2008.
(46) Lammps, http://www.cs.sandia.gov/~sjplimp /lammps.html, 2006.
(47) Foiles, S. M.; Baskes, M. I.; Daw, M. S. *Phys. Rev. B* **1986**, *33*, 7983–7991.
(48) Wan, J.; Fan, Y. L.; Gong, D. W.; Shen, S. G.; Fan, X. Q. *Modell. Simul. Mater. Sci. Eng.* **1999**, *7*, 189–206.
(49) Sun, C. Q.; Tay, B. K.; Zeng, X. T.; Li, S.; Chen, T. P.; Zhou, J.; Bai, H. L.; Jiang, E. Y. *J. Phys.: Condens. Matter* **2002**, *14*, 7781–7795.
(50) McMahon, J. M.; Gray, S. K.; Schatz, G. C. *Phys. Rev. Lett.* **2009**, *103*, 097403.
(51) Pack, A.; Hietschold, M.; Wannemacher, R. *Opt. Commun.* **2001**, *194*, 277−287.
(52) Chang, R.; Leung, P. T. *Phys. Rev. B* **2006**, *73*, 125438.
(53) Palomba, S.; Novotny, L.; Palmer, R. *Opt. Commun.* **2008**, *281*, 480–483.
(54) de Abajo, F. J. G. *J. Phys. Chem. C* **2008**, *112*, 17983–17987.
(55) Fedrigo, S.; Harbich, W.; Buttet, J. *Phys. Rev. B* **1993**, *47*, 10706–10715.
(56) Kresin, V. V. *Phys. Rev. B* **1995**, *51*, 1844–1849.
(57) Ekardt, W. *Phys. Rev. B* **1985**, *31*, 6360–6370.
(58) Palpant, B.; Prevel, B.; Lerme, J.; Cottancin, E.; Pellarin, M.; Treilleux, M.; Perez, A.; Vialle, J. L.; Broyer, M. *Phys. Rev. B* **1998**, *57*, 1963–1970.

JP100456P